Weyl points in multiterminal hybrid superconductor-semiconductor nanowire devices

Repin, E. V.; Nazarov, Y. V.

DOI
10.1103/PhysRevB.105.L041405

Publication date
2022

Document Version
Final published version

Published in
Physical Review B

Letter | Editors' Suggestion

Weyl points in multiterminal hybrid superconductor-semiconductor nanowire devices

E. V. Repin and Y. V. Nazarov
Kavli Institute of Nanoscience, Delft University of Technology, 2628 CJ Delft, The Netherlands

(Received 22 October 2020; accepted 8 December 2021; published 12 January 2022)

The technology of superconductor-semiconductor nanowire devices has matured in recent years. This makes it feasible to make more complex and sophisticated devices. We investigate multiterminal superconductor-semiconductor wires to access the feasibility of another topological phenomenon: Weyl singularities in their spectrum. We have found an abundance of Weyl singularities for devices with an intermediate size of the electrodes. We describe their properties and the ways the singularities emerge and disappear upon variation of the setup parameters.

DOI: 10.1103/PhysRevB.105.L041405

The topological properties of solids have been a subject of intense research for many years [1,2]. Prominent examples of topological materials include topological superconductors [3] that may host Majorana modes [4] and Weyl semimetals [5] with Weyl points [6] in the electron spectrum. Despite big interest, the fabrication, purification, and experimental analysis of topological materials are difficult and challenging [7]. This has motivated a large effort to realize topologically nontrivial quantum states with topologically trivial materials [4,7].

The most well known and successful effort of this kind is the realization of zero-energy Majorana states, which can be useful in topological quantum computing [8] and in semiconductor nanowires covered by superconducting electrodes, so-called hybrid superconductor-semiconductor nanowire devices. The first experimental observation [9] came only two years after the first theoretical proposal [10], yet considerable enhancement of the technology was needed for further progress. With the achievement of ballistic superconductivity [11] and experimental verification of topological signatures in the Josephson effect [12], the very active subfield and technologies in use are mature enough for the next level of experimental sophistication [13,14]. One of the interesting directions is the fabrication of multiterminal nanowire-based devices [13]. Recently proposed Andreev molecules [15] that exhibit nontrivial features in the spectrum of Andreev states [16,17] require three superconducting terminals, and fabrication efforts are underway. In the same manner, one can realize devices with more terminals.

It has been suggested that topologically protected spectral singularities—Weyl points—may be realized in multiterminal superconducting nanostructures [18], potentially in any nanostructure. The tuning of three parameters is required to achieve the singularity, so the minimum number of terminals is four, corresponding to three independent superconducting phases. The singularity is pinned to zero energy (counted from the Fermi level) in the absence of spin-orbit interaction and is at the finite-energy distance if spin-orbit interaction is significant [19]. The topological charge is manifested by transconductance quantization [18,20] and can be detected by a spectroscopic measurement [21], with some complications brought by the continuous spectrum above the superconducting gap [22]. Four-terminal devices have been fabricated in graphene [23] and two-dimensional (2D) semiconducting structures [24]. However, the experimental confirmation of Weyl points is not yet available. The presence or absence of Weyl points in any concrete nanostructure depends on details of scattering that may be difficult to identify and control, and only 6% of random scattering matrices provide those. To facilitate the experimental observation and possible applications, it would be good to propose a system where the Weyl points are relatively abundant.

In this Letter, we investigate the presence of Weyl points in the spectrum of a single-nanowire four-terminal hybrid semiconducting device with a straightforward design and, indeed, find many of those. Our setup is distinct from a widely investigated one where several nanowires with zero-energy Majorana modes at their ends are brought close to each other to provide the tunneling between the ends [25–30]. In fact, we look for Weyl points at finite energy, where they are present irrespective of the Majorana modes, and find them in both topologically trivial and nontrivial wires [31].

A typical spectrum with a Weyl point is presented in Fig. 1. We set $\phi_{1,2}$ in such a way that the line passes the Weyl point. The other feature of the spectrum is the zero-energy crossing (ZEC) [19,32] that occurs at a 2D surface in the three-dimensional (3D) space of phases. If the wire is in the nontopological regime, there is an even number of ZECs separating the regions with different parities of the ground state. If, as in Fig. 1, the wire is in the topological regime, the number of crossings may be odd [10], manifesting so-called 4π periodicity. The parity determination requires consideration of the zero-energy state at the far ends of the wire [33].

We concentrate on a family of setups where a (formally infinite) semiconducting nanowire is covered by four separate superconducting films (see Fig. 1). The films are the superconducting leads kept at the corresponding superconducting phases $\phi_0 = 0, \phi_{1,2,3}$. The widths of two intermediate leads $s_{1,2}$ and the gaps between the leads $g_{1,2,3}$ sum up to L. A setup

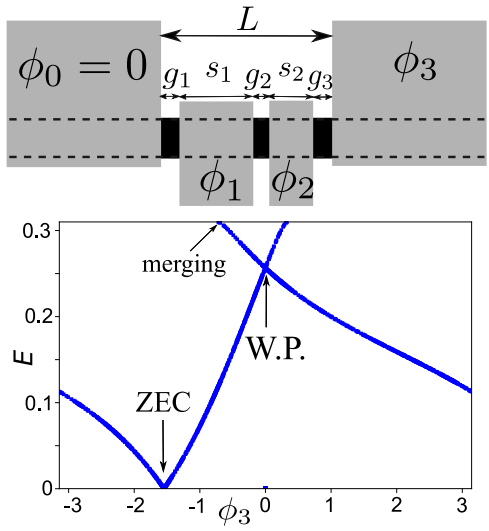

FIG. 1. Top: The family of hybrid superconductor-semiconductor setups under consideration. A long semiconducting nanowire is covered by four superconducting leads kept at three independent superconducting phases $\phi_{1,2,3}$. A setup is characterized by overall length L and the lengths of electrodes and gaps, $s_{1,2}$ and $g_{1,2,3}$. Bottom: A typical spectrum of Andreev bound states along the line passing a Weyl point where the bands cross. Other features worth attention are the zero-energy crossing that occurs at a 2D surface in the 3D space of the phases and merging of the second energy band with the gap edge (top edge of the plot).

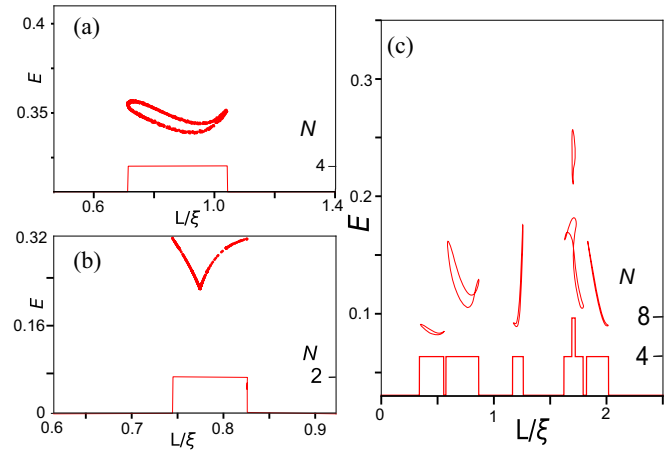

FIG. 2. Number and energy dependence of Weyl points for several setups. Nontopological regime: (a) $\mu, B, |\Delta| = (1, 1, 2)$, $\xi \approx 1.07$, $\vec{s} = (0, 0.7, 0, 0.3, 0.0)$ and (b) $\mu, B, |\Delta| = (1, 1, 0.9)$, $\xi \approx 2.30$, $\vec{s} = (0.04, 0.61, 0.09, 0.26, 0)$. Topological regime: (c) $\mu, B, |\Delta| = (0.464, 1.144, 0.693)$, $\xi \approx 3.26$. For (b) and (c), the gap edge is at the top edge of the plot. For (a), the gap edge is at 1.24.

of the family is thus characterized by L and five numbers, $\vec{s} \equiv [g_1/L, s_1/L, g_2/L, s_2/L, g_3/L]$, summing to 1. We investigate the possibility to realize Weyl points in the three-dimensional phase space of three superconducting phases with varying L.

The wave function of an Andreev bound state is localized at a typical scale ξ that will be precisely defined below. At $L \ll \xi$ we expect no Weyl points since in this case the localized state hardly feels the middle leads and its energy depends on only a single parameter, $E(\phi_3)$. Neither do we expect the Weyl points in the opposite limit $L \gg \xi$: in this case, the states are localized in the corresponding gaps g_i with the energies depending on the local phase differences $\phi_i - \phi_{i-1}$, again depending on a single parameter each. Therefore, we expect Weyl points to appear for each setup at $L \sim \xi$. Indeed, for most choices of $\vec{s}$ we find one or more intervals of L where the Weyl points are present in both the topological and nontopological regimes.

We employ the Lutchin-Sau-Das-Sarma Hamiltonian [10]:

$$H = \left(\frac{p^2}{2} - p\sigma_z - \mu\right)\tau_z + \mathrm{Re}\Delta(x)\tau_x + \mathrm{Im}\Delta(x)\tau_y + B\sigma_x, \tag{1}$$

which we made dimensionless by measuring lengths and energies in units of spin-orbit length and spin-orbit energy, with τ_i and σ_i being Pauli matrices in Nambu and spin space, respectively. Here, $\Delta(x)$ is the superconducting order parameter induced in the wire. We assume a piecewise-constant spatial dependence where $\Delta(x) = |\Delta|e^{i\phi_i}$ under the leads, with ϕ_i being the phase of the corresponding lead and $\Delta(x) = 0$ within the gaps (see Fig. 1). The wire is in the topological regime [10] provided that $|B| > \sqrt{|\Delta|^2 + \mu^2}$; otherwise, it is in the nontopological one.

We stress that this is a minimal model. More extensive modeling would bring the regular variation of μ to account for the doping by electrodes and irregular variation of μ to account for disorder and possibly would incorporate more one-dimensional modes. All this may modify the extent and details of localized wave functions but not our main qualitative conclusion: Weyl points appear when the extent of the wave functions ξ is of the order of L.

The Hamiltonian (1) possesses the usual Bogoliubov–de Gennes symmetry $H^* = -\sigma_y\tau_y H \tau_y\sigma_y$ that guarantees the symmetry of the spectrum and Weyl points with respect to $E \to -E$. We concentrate on positive energies. Although the Hamiltonian (1) is not invariant with respect to time reversal, there is a look-alike extra symmetry,

$$H^*(\vec{\phi}) = \sigma_x H(-\vec{\phi})\sigma_x, \tag{2}$$

relating the Hamiltonians at opposite points $\vec{\phi}$ and $-\vec{\phi}$ in phase space. Therefore, the Weyl points come in pairs of the same charge at opposite points, like for a time-reversible scattering matrix [18]. It was suggested in [18] that Weyl points always emerge in groups of four to conform to the conservation of topological charge. Here, we find notable exceptions from this rule: Weyl points emerging from the continuous spectrum at the gap edge.

The relevant examples of our numerical results are presented in Figs. 2–4. In Fig. 2 we plot the number and energies of the Weyl points versus the overall setup length L. For each parameter set μ, $|\Delta|$, and B we compute the localization length ξ defined as the slowest decaying exponent under the outer leads at zero energy. So-defined ξ is hard to express analytically, although it is the best estimation of the wave function extent. We measure L in units of ξ. For all parameters and setups investigated, we find Weyl points in one or several intervals around $L \simeq \xi$. We observe strong dependence of the

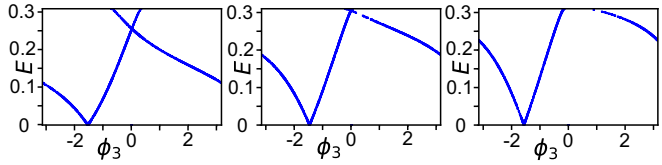

FIG. 3. Merging of a Weyl point with the gap edge. The choice of the parameters and setup is the same as in Fig. 2(c). We plot the spectrum versus ϕ_3 at a line hitting the Weyl point for three values of L. Left: $L/\xi = 0.781$, $\phi_1 = 2.639$, $\phi_2 = 2.629$, the Weyl point is $E = 0.256$, and $\phi_3 = 0.002$. Middle: $L/\xi = 0.824$, $\phi_1 = 2.260$, $\phi_2 = 2.256$, and the Weyl point is precisely at the gap edge $E_g = 0.31$. Right: $L/\xi = 0.829$; there is no Weyl point, and no bound state is found in an interval of ϕ_3.

number and energy dependences on the setup details. This is explained by the fact that the Weyl points emerge from complex interference in the setup, with the interference pattern being affected by all details.

In the nontopological regime [Figs. 2(a) and 2(c)] the points come in groups of four. Their energy dependence is seen to be a closed curve, a trajectory in L-E space, that does not touch the gap edge. The curves may intersect or self-intersect, with the intersection corresponding to points at the same energy but separated in phase space. The number of Weyl points at a given L is 2 times the number of intersections of the line $L = \text{const}$ with all the curves, as we see in the plots. Let us discuss the emergence of Weyl points upon changing L, taking Fig. 2(a) as an example. There are no points at $L < 0.71$. At $L = 0.71$, a pair of close points of opposite topological charges emerges at some phase settings $\vec{\phi}$, with

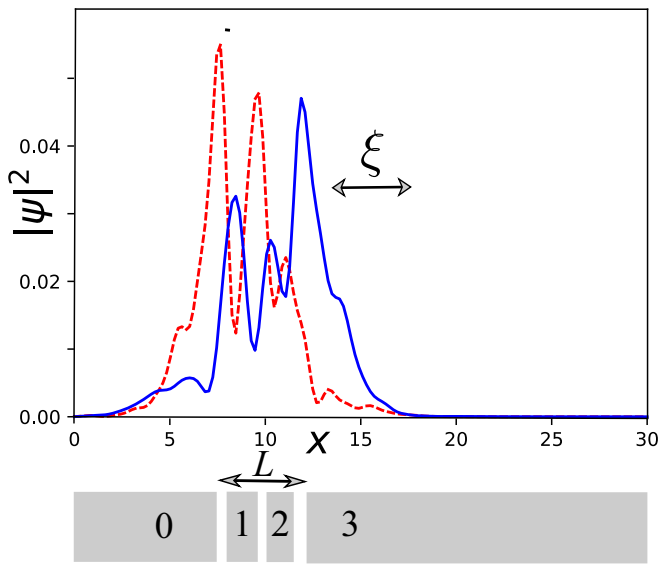

FIG. 4. The densities $\sum_i |\psi(x)|_i^2$ of two degenerate wave functions (solid and dashed curves) at a Weyl point. The wave functions in the degenerate subspace are chosen to be eigenvectors of the coordinate operator x. The calculations are made for a finite wire of total length $l = 30$, the overlaps with leads 0–3 are shown below the plot. The parameters are $B, \mu, |\Delta| = (1, 1, 0.9)$, corresponding to $\xi = 4.0$, $\vec{s} = (1/9, 1/3, 1/9, 1/3, 1/9)$. For $L = 4.5$, the point is found at $\phi_1, \phi_2, \phi_3 = (3.059, -0.448, 1.631)$.

close energies. At the same L, another pair emerges near $-\vec{\phi}$, so four points appear in total. Upon changing L up to 0.9, the points get separated in phase settings and energy. As explained in [18,19], any 2D plane that separates the points in the phase space acquires a nontrivial Chern number that is manifested as a quantized transconductance at even parity of the setup. Upon a further change in L, the points with opposite charges get close together and eventually annihilate at $L = 1.04$. All this is seen as a closed trajectory in L-E space. A more complex picture involving multiple trajectories of the same kind (let us call those type A trajectories) is seen in Fig. 2(b).

In the topological regime, zero-energy states are formed at the far ends of the wire (this is not detected in our approach, which concentrates on the states localized at all electrodes). An example is provided in Fig. 2(b). There are no points for $L < 0.745$. At $L = 0.745$, a Weyl point emerges from the continuous spectrum at some phase setting ϕ. The symmetry implies that another point of the same topological charge emerges at $-\phi$, so two points appear in total. Upon changing L the point changes its phase coordinate. It gets lower in energy first but eventually returns back to the gap edge and disappears at $L = 0.781$. Such trajectories begin and end at the gap edge: let us call those type B trajectories.

We stress that such merging is not compatible with the presence of a continuous band of localized states throughout the Brillouin zone. This is seen from the following topological argument. Let us consider a 2D plane far from the point where the merging occurs. If there is a continuous band throughout the plane, the Chern number is well defined. However, it must change upon merging. Since the plane is far from the merging point, this is impossible and proves the absence of such a band, which also implies the absence of quantized transconductance. Indeed, a detailed view of the spectrum near where the Weyl point merges (Fig. 3) shows that the localized states merge with a continuous spectrum, and there are regions in the Brillouin zone where no localized state is present.

In total, we have investigated 12 setups, an equal number in the topological and nontopological regimes. Ten of them have Weyl points in the interval of $L \simeq \xi$. In several cases, we were not able to trace the whole curve and identify its type. Our observation is that we have seen the type B trajectory in only the topological regime. However, no fundamental topological restriction can forbid type B trajectories in the nontopological regime or type A trajectories in the topological regime. One can see that if one considers a long but finite wire where the overall spectrum is discrete. Such regularization affects only the states at very small energies. For discrete spectrum, all trajectories are of type A. Presently, we assume that the observation is valid for the specific family of setups under consideration and is explained by the fact that the boundary conditions near the gap edge in the topological regime are more favorable for merging the localized states with the continuum. More detailed research is underway.

We illustrate the wave functions of the localized states at a Weyl point in Fig. 4. The specifics of the situation are that there are two degenerate wave functions at the point, so eventually we could plot any linear combination of the two. The choice made is as follows: we consider matrix elements of the coordinate operator x in two-dimensional degenerate subspace and determine and plot the corresponding eigenfunctions.

The resulting eigenfunctions are therefore maximally separated in coordinate. We observe the localization of the wave functions at several ξ at the setup and a complex multiple-peak structure that witnesses complex wave interference required for Weyl points. The setup chosen has mirror symmetry that is, however, violated by nonsymmetric phase settings. Still, the wave functions look approximately mirror symmetric.

To conclude, we have investigated the occurrence of Weyl points in the spectrum of Andreev bound states in a family of realistic device setups where a semiconducting nanowire is covered by four superconducting electrodes. It is feasible to realize such setups experimentally and observe the corresponding topological singularities. For most setups, we find Weyl points for $L \simeq \xi$, that is for a setup length of the order of the localization length of the bound states. In experiments, *in situ* control of the device length is not feasible. However, it is custom for such devices to utilize a set of gate electrodes to control $\mu(x)$. We believe that this permits tuning the device to the region where Weyl points are present.

We observed two types of Weyl point trajectories. The type A trajectories do not touch the gap edge, and the Weyl points appear in groups of four. For type B trajectories, the Weyl points emerge from the gap edge in pairs. We found the type B trajectory in only the topological regime; this should be specific for the family of setups under consideration.

We acknowledge useful discussions with M. Houzet and J. Meyer. This research was supported by the European Research Council (ERC) under the European Union's Horizon 2020 research and innovation program (Grant Agreement No. 694272).

[1] X. Qi and S. Zhang, Rev. Mod. Phys. **83**, 1057 (2011).
[2] B. Bernevig, T. Hughes, and S. Zhang, Science **314**, 1757 (2006).
[3] M. Sato and Y. Ando, Rep. Prog. Phys. **80**, 076501 (2017).
[4] J. Alicea, Rep. Prog. Phys. **75**, 076501 (2012).
[5] N. P. Armitage, E. J. Mele, and A. Vishwanath, Rev. Mod. Phys. **90**, 015001 (2018).
[6] H. Weyl, Z. Phys. **56**, 330 (1929).
[7] P. Liu, J. R. Williams, and J. J. Cha, Nat. Rev. Mater. **4**, 479 (2019).
[8] C. Nayak, S. H. Simon, A. Stern, M. Freedman, and S. Das Sarma, Rev. Mod. Phys. **80**, 1083 (2008).
[9] V. Mourik, K. Zuo, S. M. Frolov, S. R. Plissard, E. P. A. M. Bakkers, and L. P. Kouwenhoven, Science **336**, 1003 (2012).
[10] R. M. Lutchyn, J. D. Sau, and S. Das Sarma, Phys. Rev. Lett. **105**, 077001 (2010).
[11] H. Zhang *et al.*, Nat. Commun. **8**, 16025 (2017).
[12] D. Laroche, D. Bouman, D. J. van Woerkom, A. Proutski, C. Murthy, D. I. Pikulin, C. Nayak, R. J. J. van Gulik, J. Nygard, P. Krogstrup, L. P. Kouwenhoven, and A. Geresdi, Nat. Commun. **10**, 245 (2019).
[13] H. Zhang, D. E. Liu, M. Wimmer, and L. P. Kouwenhoven, Nat. Commun. **10**, 5128 (2019).
[14] S. M. Frolov, M. J. Manfra, and J. D. Sau, Nat. Phys. **16**, 718 (2020).
[15] J. D. Pillet, V. Benzoni, J. Griesmar, J. L. Smirr, and C. O. Girit, Nano Lett. **19**, 7138 (2019).
[16] V. Kornich, H. S. Barakov, and Y. V. Nazarov, Phys. Rev. Res. **1**, 033004 (2019).
[17] V. Kornich, H. S. Barakov, and Y. V. Nazarov, Phys. Rev. B **101**, 195430 (2020).
[18] R.-P. Riwar, M. Houzet, J. S. Meyer, and Y. V. Nazarov, Nat. Commun. **7**, 11167 (2016).
[19] T. Yokoyama and Y. V. Nazarov, Phys. Rev. B **92**, 155437 (2015).
[20] E. Eriksson, R.-P. Riwar, M. Houzet, J. S. Meyer, and Y. V. Nazarov, Phys. Rev. B **95**, 075417 (2017).
[21] R. L. Klees, G. Rastelli, J. C. Cuevas, and W. Belzig, Phys. Rev. Lett. **124**, 197002 (2020).
[22] E. V. Repin, Y. Chen, and Y. V. Nazarov, Phys. Rev. B **99**, 165414 (2019).
[23] A. W. Draelos, M.-T. Wei, A. Seredinski, H. Li, Y. Mehta, K. Watanabe, T. Taniguchi, I. V. Borzenets, F. Amet, and G. Finkelstein, Nano Lett. **19**, 1039 (2019).
[24] N. Pankratova, H. Lee, R. Kuzmin, K. Wickramasinghe, W. Mayer, J. Yuan, M. G. Vavilov, J. Shabani, and V. E. Manucharyan, Phys. Rev. X **10**, 031051 (2020).
[25] K. Sakurai, M. T. Mercaldo, S. Kobayashi, A. Yamakage, S. Ikegaya, T. Habe, P. Kotetes, M. Cuoco, and Y. Asano, Phys. Rev. B **101**, 174506 (2020).
[26] J. P. T. Stenger and D. Pekker, Phys. Rev. B **100**, 035420 (2019).
[27] M. Houzet and J. S. Meyer, Phys. Rev. B **100**, 014521 (2019).
[28] L. Peralta Gavensky, G. Usaj, and C. A. Balseiro, Phys. Rev. B **100**, 014514 (2019).
[29] J. S. Meyer and M. Houzet, Phys. Rev. B **103**, 174504 (2021).
[30] M. Alvarado, A. Iks, A. Zazunov, R. Egger, and A. L. Yeyati, Phys. Rev. B **101**, 094511 (2020).
[31] See Supplemental Material at http://link.aps.org/supplemental/10.1103/PhysRevB.105.L041405 for a detailed explanation of our numerical calculations.
[32] B. van Heck, S. Mi, and A. R. Akhmerov, Phys. Rev. B **90**, 155450 (2014).
[33] D. I. Pikulin and Y. V. Nazarov, Phys. Rev. B **86**, 140504(R) (2012).